Biogeosciences Discuss., 4, 1877–1921, 2007
www.biogeosciences-discuss.net/4/1877/2007/

Biogeosciences Discussions

Biogeosciences Discussions is the access reviewed discussion forum of *Biogeosciences*

Spatio-temporal variability of marine primary and export production in three global coupled climate carbon cycle models

B. Schneider[1], L. Bopp[1], M. Gehlen[1], J. Segschneider[2], T. L. Frölicher[3], F. Joos[3], P. Cadule[1], P. Friedlingstein[1], S. C. Doney[4], and M. J. Behrenfeld[5]

[1]Laboratoire du Climat et de l'Environnement (LSCE), L'Orme des Merisiers Bât. 712, 91191 Gif sur Yvette, France
[2]Max-Planck-Institut für Meteorologie, Bundesstrasse 55, 20146 Hamburg, Germany
[3]Climate and Environmental Physics, Physics Institute, University of Bern, Sidlerstrasse 5, 3012 Bern, Switzerland
[4]Department of Marine Chemistry and Geochemistry, Woods Hole Oceanographic Institution, Woods Hole, MA 02543-1543, USA
[5]Department of Botany and Plant Pathology, Cordley Hall 2082, Oregon State University, Corvallis, OR 97331-2902, USA

Received: 7 June 2007 – Accepted: 7 June 2007 – Published: 22 June 2007

Correspondence to: Birgit Schneider (birgit.schneider@lsce.ipsl.fr)

Abstract

This study compares spatial and temporal variability in net primary productivity (PP) and particulate organic carbon (POC) export production (EP) from three different coupled climate carbon cycle models (IPSL, MPIM, NCAR) with observation-based estimates derived from satellite measurements of ocean colour and inverse modelling. Satellite observations of ocean colour have shown that temporal variability of PP on the global scale is largely dominated by the permanently stratified, low-latitude ocean (Behrenfeld et al., 2006) with stronger stratification (higher SSTs) leading to negative PP anomalies and vice versa. Results from all three coupled models confirm the role of the low-latitude, permanently stratified ocean for global PP anomalies. Two of the models also reproduce the inverse relationship between stratification (SST) and PP, especially in the equatorial Pacific. With the help of the model results we are able to explain the chain of cause and effect leading from stratification (SST) through nutrient concentrations to PP and finally to EP. There are significant uncertainties in observational PP and especially EP. Our finding of a good agreement between independent estimates from coupled models and satellite observations provides increased confidence that such models can be used as a first basis to estimate the impact of future climate change on marine productivity and carbon export.

1 Introduction

Marine net primary productivity (PP) is a key process in the global carbon cycle, controlling the uptake of dissolved inorganic carbon (DIC) in the sunlit surface waters of the ocean and its transfer into organic carbon (OC). Subsequent gravitational sinking of detrital particulate organic carbon (POC) through the water column results in the export of POC (EP) from the surface into the ocean's interior, where it becomes partly or entirely remineralised and eventually transported back to the surface. The export of organic matter leads to a depletion in DIC and nutrients in the surface and an enrich-

ment in the deep. Without this biological cycle, surface water pCO_2 and consequently atmospheric CO_2 would be higher than observed (Volk and Hoffert, 1985). However, neither absolute values for global annual PP and EP nor their spatial and temporal variability are well known from observations. Changes in ocean circulation and nutrient cycling, as they will occur as a consequence of climate change, will impact PP and EP differently, demanding a better understanding of the mechanisms involved.

Satellite measurements of ocean colour have been used to derive surface water chlorophyll concentrations (Chl), carbon biomass and PP (Behrenfeld et al., 2006, 1997; Carr et al., 2006). These methods have the advantage in that they provide large spatial and temporal coverage of vast ocean areas. Reference measurements from ship-based observations, however, are still sparse. Complex algorithms lead stepwise from ocean colour measurements to Chl concentrations, and from Chl, light, and temperature to PP and sometimes even further to EP estimates. These include a number of assumptions concerning, for example, vertical and temporal resolution of the parameters to be determined, which increases the uncertainty for the results obtained after each step. For example, Carr et al. (2006) examined results from 24 different methods to determine PP from ocean colour and 7 general circulation models (GCMs), finding a factor of two difference between global bulk estimates for PP, that range from 35 to 70 GtC/yr. Nevertheless, patterns of spatial and temporal variability of PP are similar between different approaches, giving a first indication of the spatio-temporal variability of PP.

Export fluxes of organic carbon (OC) are even harder to constrain than PP. They are difficult to be measured directly and in some approaches have to be referred to a certain depth level, which is defined differently across studies (Oschlies and Kähler, 2004; Laws et al., 2000; Schlitzer, 2000). This complicates the comparison of such results. Observation-based estimates suggest that global POC export production is in the range of 11 to 22 GtC/yr (Laws et al, 2000; Schlitzer et al., 2000; Eppley and Peterson, 1979).

Ocean circulation and mixing is an important governing factor for biological produc-

tivity and organic matter export. It controls the transport of nutrients into the euphotic zone and thus nutrient availability for marine biological production. Najjar et al. (2007) found that the global carbon export (POC and DOC) varied from 9 to 28 GtC/yr in 13 different ocean circulation models using the same biogeochemical model (OCMIP-2). The importance of realistic physics has also been highlighted by Doney et al. (2004) using the same ocean models. The export of organic matter is, however, an important quantity to constrain as it describes the amount of OC that is transported from the surface ocean to depth, causing a vertical gradient of dissolved inorganic carbon (DIC) in the water column (Volk and Hoffert, 1985). Potential changes in export may change the uptake of anthropogenic carbon from the atmosphere.

A quantitative understanding of the processes that control PP and EP and their implementation in coupled climate biogeochemical models is essential to project the effect of future climate change on marine productivity, carbon export fluxes (Bopp et al., 2005; Plattner et al., 2001; Joos et al.,1999; Maier-Reimer et al., 1996) and their possible feedbacks on the climate system (Friedlingstein et al., 2006). Unfortunately, productivity and export are not well constrained by observations, making it difficult to validate corresponding results from climate models. Productivity estimates from coupled models and satellite observations are to a large degree independent in construction, and cross-comparison of the two approaches provides a promising way to assess jointly their overall skill and identify the main underlying mechanisms that control PP and EP variability. To do so, this study investigates results from three different fully coupled climate carbon cycle models (IPSL, MPIM, NCAR) that include interactions between the atmosphere, ocean circulation and sea-ice, marine biogeochemical cycles and the terrestrial biosphere. As all three models differ in their major components (atmosphere, ocean, terrestrial and marine biospheres), the aim of this study is to give a description of the present day situation of marine PP and EP as simulated by coupled models. Note that it would not be sufficient to investigate the primary and export production in a (far cheaper) set of forced ocean-only model experiments, since climate in the fully coupled models (e.g. ocean currents and resulting nutrient distributions, cloud cover

and resulting insolation) will most likely differ from any reanalysed state.

Modelled circulation fields are compared with observations of temperature (T), salinity (S), mixed layer depth (MLD) and water mass transports of the Atlantic Meridional Overturning Circulation (AMOC). To assess the models' capability to reproduce El Nino Southern Oscillation (ENSO) variability, maximum entropy power spectra of sea surface temperatures (SST) from the equatorial Pacific are computed. The representation of marine biogeochemical cycles is assessed by comparing modelled with observed PO_4 concentrations, which in the current study are fully prognostic in contrast to the former model simulations of the OCMIP-2 study, where PO_4 was restored (Najjar et al., 2007). The evaluation of PP covers global annual mean fields, global integrals, seasonal cycle and interannual variability. We compare model results with PP derived from satellite measurements of ocean colour and explain the main mechanisms causing interannual variability of simulated PP. Global annual mean fields and global integrals for EP from the models are also compared with observation-based estimates. Thereby, we identify regions where EP reacts most sensitive to interannual climate variability. The present day situation of PP and EP from our results can be taken as a basis for a first guess of the impact of future climate change on marine PP and EP, which will be investigated in more detail in a complementary study.

2 Methodology

2.1 Data sets

Results for temperature (T), salinity (S) and PO_4 distributions are compared with observed climatological values from the World Ocean Atlas (WOA; Collier and Durack, 2006; Conkright et al., 2002) to assess the reliability of modelled ocean circulation fields and biogeochemical cycles. Furthermore, the representation of the maximum mixed layer depth, which is a dynamically important variable for water mass formation, light limitation, and nutrient entrainment, is assessed by comparison with observations

from Boyer-Montégut et al. (2004). Modelled fields of PP are compared with PP derived from ocean colour (Behrenfeld et al., 2006) (http://web.science.oregonstate.edu/ocean.productivity/onlineVgpmSWData.php) and EP distributions are compared with results from (inverse) modelling, which refer to a depth of 133 m (Schlitzer, 2000) and 100 m (Laws et al., 2000), respectively. As neither for PP nor for EP approriate in-situ data are available, the latter is rather a comparison between different models.

2.2 Models

All models used in this study consist of fully coupled 3-D atmosphere-ocean climate models that have also contributed to the IPCC Fourth Assessment Report (AR4; Solomon et al., 2007; Meehl et al., 2007). The models were run with additional carbon cycle modules for the terrestrial and oceanic biospheres (Friedlingstein et al., 2006).

2.2.1 IPSL

The IPSL-CM4-LOOP (IPSL) model consists of the Laboratoire de Météorologie Dynamique atmospheric model (LMDZ-4) with a horizontal resolution of about $3^\circ \times 3^\circ$ and 19 vertical levels (Hourdin et al., 2006), coupled to the OPA-8 ocean model with a horizontal resolution of $2^\circ \times 2^\circ \cdot \cos\phi$ and 31 vertical levels and the LIM sea ice model (Madec et al., 1998). The terrestrial biosphere is represented by the global vegetation model ORCHIDEE (Krinner et al., 2005), the marine carbon cycle by the PISCES model (Aumont et al., 2003). PISCES simulates the cycling of carbon, oxygen and the major nutrients determining phytoplankton growth (PO_4, NO_3, NH_4, Si, Fe). Phytoplankton growth is limited by the availability of nutrients, temperature and light. The model has two phytoplankton size classes (small and large), representing nanophytoplankton and diatoms, as well as two zooplankton size classes (small and large), representing microzooplankton and mesozooplankton. For all species the C:N:P ratios are assumed constant (122:16:1), while the internal ratios of Fe:C, Chl:C and Si:C of phytoplankton are predicted by the model. There are three non-living components

of organic carbon in the model: semi-labile dissolved organic carbon (DOC), with a lifetime of several weeks to years, as well as large and small detrital particles, which are fueled by mortality, aggregation, fecal pellet production and grazing. Small detrital particles sink through the water column with a constant sinking speed of 3 m/day, while for large particles the sinking speed increases with depth from a value of 50 m/day at the depth of the mixed layer, increasing to a maximum sinking speed of 425 m/day at 5000 m depth. For a more detailed description of the PISCES model see Amount and Bopp (2006) and Gehlen et al. (2006). Further details and results from the fully coupled model simulation of the IPSL-CM4-LOOP model are given in Friedlingstein et al. (2006).

2.2.2 MPIM

The Earth System Model employed at the Max-Planck-Institut für Meteorologie (MPIM) consists of the ECHAM5 (Roeckner et al., 2006) atmospheric model in T63L31 resolution with embedded JSBACH terrestrial biosphere model and the MPIOM physical ocean model, which further includes a sea-ice model (Marsland et al., 2003) and the HAMOCC5.1 marine biogeochemistry model (Maier-Reimer et al., 2005). The coupling of the marine and atmospheric model components, and in particular the carbon cycles is achieved by using the OASIS coupler.

HAMOCC5.1 is implemented into the MPIOM physical ocean model (Marsland et al., 2003) using a curvilinear coordinate system with a 1.5° nominal resolution where the North Pole is placed over Greenland, thus providing relatively high horizontal resolution in the Nordic Seas. The vertical resolution is 40 layers, with higher resolution in the upper part of the water column (10 m at the surface to 13 m at 90 m). The marine biogeochemical model HAMOCC5.1 is designed to address large scale/long term features of the marine carbon cycle, rather than to give a complete description of the marine ecosystem. Consequently, HAMOCC5.1 is a NPZD model with two phytoplankton types (opal and calcite producers) and one zooplankton species. The carbonate chemistry is identical to the one described in Maier-Reimer (1993). A more detailed

description of HAMOCC5.1 can be found in Maier-Reimer et al. (2005), while here only the main features relevant for the described experiments will be outlined.

Marine biological production is limited by the availability of phosphorous, nitrate and iron. Silicate concentrations are used to distinguish the growth of diatoms and coccolithophorides: if silicate is abundant, diatoms grow first, thereby reducing the amount of nutrients available for coccolithophoride growth. The production of calcium carbonate shells occurs in a fixed ratio of the phytoplankton growth (0.2). The model also includes cyanobacteria that take up nitrogen from the atmosphere and transform it immediately into nitrate. Please note that biological production is temperature-independent, assuming that phytoplankton acclimate to local conditions. Global dust deposition fields are used to define the source function of bioavailable iron. Removal of dissolved iron occurs through biological uptake and export and by scavenging, which is described as a relaxation to the deep ocean iron concentration of 0.6 nmol/m^3. In the experiments used here, export of particulate matter is simulated using prescribed settling velocities for opal (30 m/day), calcite shells (30 m/day) and organic carbon (10 m/day). Remineralisation of organic matter depends on the availability of oxygen. In anoxic regions, remineralisation using oxygen from denitrification takes place.

HAMOCC5.1 also includes an interactive module to describe the sediment flux at the sea floor. This component simulates pore water chemistry, the solid sediment fraction and interactions between the sediment and the oceanic bottom layer as well as between solid sediment and pore water constituents.

2.2.3 NCAR

The physical core of the NCAR CSM1.4 carbon climate model (Doney et al., 2006; Fung et al., 2005) is a modified version of the NCAR CSM1.4 coupled physical model, consisting of ocean, atmosphere, land and sea-ice components integrated via a flux coupler without flux adjustments (Bolville et al., 2001; Bolville and Gent, 1998). The atmospheric model CCM3 is run with a spectral truncation resolution of 3.75° (T31) and 18 levels in the vertical (Kiehl et al., 1998). The ocean model is the NCAR CSM Ocean

Model (NCOM) with 25 levels in the vertical and a resolution of 3.6° in longitude and 0.8° to 1.8° in latitude (T31×3) (Gent et al., 1998). The water cycle is closed through a river runoff scheme, and modifications have been made to the ocean horizontal and vertical diffusivity's and viscosity's from the original version (CSM1.0) to improve the equatorial ocean circulation and interannual variability. The sea ice component model runs at the same resolution as the ocean model, and the land surface model runs at the same resolution as the atmospheric model.

The CSM1.4-carbon model includes a modified version of the terrestrial biogeochemistry model CASA (Carnegie-Ames-Stanford Approach) (Randerson et al., 1997), and a derivate of the OCMIP-2 (Ocean Carbon-Cycle Model Intercomparison Project Phase 2) oceanic biogeochemistry model (see Najjar, R. G. and Orr, J. C., 1999, unpublished manuscript, OCMIP-2 Biotic-HOWTO; available online at http://www.ipsl.jussieu.fr/OCMIP/). In the ocean model the biological source-sink term has been changed from a nutrient restoring formulation to a prognostic formulation, thus biological productivity is modulated by temperature, surface solar irradiance, mixed layer depth, and macro- and micronutrients. Following the OCMIP-2 protocols (Najjar et al., 2007), total biological productivity is partitioned 1/3 into sinking POC flux, equivalent to EP, and 2/3 into the formation of dissolved or suspended organic matter, much of which is remineralised within the model euphotic zone. Total productivity thus contains both new and regenerated production, though the regenerated contribution is probably lower than in the real ocean. While not strictly equivalent to primary production as measured by ^{14}C methods, rather net nutrient uptake, NCAR PP is a reasonable proxy for the time and space variability of PP if somewhat underestimating the absolute magnitude. Please note that in this study for reasons of simplicity net nutrient uptake for NCAR is labelled and treated as PP, even though it is not essentially the same. The ocean biogeochemical model includes in simplified form the main processes of the organic and inorganic carbon cycle within the ocean, and air-sea CO_2 flux. A parameterisation of the marine iron cycle has also been introduced (Doney et al., 2006). It includes atmospheric dust deposition/iron dissolution, biological uptake, vertical parti-

cle transport and scavenging. The prognostic variables in the ocean model are phosphate (PO_4), total dissolved inorganic Fe, dissolved organic phosphorus (DOP), DIC, alkalinity and O_2. The CSM1.4-carbon source code is available electronically (see http://www.ccsm.ucar.edu/working_groups/Biogeo/csm1_bgc/) and described in detail in Doney (2006).

2.3 Experiments

All results of the current study are obtained from simulations with the coupled climate carbon cycle models explained above (IPSL, MPIM, NCAR), that simulate fully coupled interactions between the atmosphere, ocean circulation, sea-ice, marine biogeochemical cycles and terrestrial biosphere. The models are a subset of the models that contributed to the C4MIP project (Friedlingstein et al.,2006) and follow the C4MIP protocols. Two of the models (IPSL, MPIM) are only forced by the historical development of anthropogenic CO_2 emissions due to fossil fuel burning and land-use changes from preindustrial to present and the A2 scenario from the year 2000 on. In addition to that, NCAR is also forced by CH_4, N_2O, CFCs, volcanic emissions and changes in solar radiation. The ocean circulation models have been spun up for several hundreds of years, and the fully coupled versions were integrated for at least an additional one hundred years before starting the transient simulation over the industrial period from 1820 (MPIM and NCAR) and 1860 (IPSL) until the year 2100. During the time period investigated (1985–2005), the anthropogenic CO_2 emissions increase from about 7.5 to 8.6 GtC/yr, resulting in a cumulative emission of about 170 Gt of carbon during this interval. For a joint analysis of the model results and for comparison with observation-based estimates, all variables have been interpolated onto a 1°×1° grid using a gaussian interpolation and climatological mean values have been computed over the period from 1985 to 2005. This study focuses on results from those two decades to describe the present day PP and EP as obtained from coupled model simulations and observation-based estimates.

3 Results and discussion

3.1 Ocean circulation and biogeochemical cycling

In a Taylor diagram, all three models show good agreement for 3-D global annual mean distributions of temperature (Fig. 1). Global SST distributions including the seasonal cycle are even better reproduced, reaching correlation coefficients above R=0.98 and normalised standard deviations very close to 1. Salinity distributions are known to be less well reproduced by coupled climate models, which is largely attributed to deficiencies in the hydrological cycle of the atmosphere models (Schneider et al., 2007). This is also the case for the models of the current study. However, correlation coefficients for both the global annual mean 3-D salinity distributions and the SSS values including the seasonal cycle are still on the order of R=0.78–0.90. In contrast to temperature, the agreement between modelled and observed salinity distributions is poorer when going from the global annual mean 3-D field to seasonal surface water values, which is due to a stronger influence of possible misfits from the atmospheric hydrological cycle, as mentioned above. While correlation coefficients remain similar, the normalised standard deviations are considerably higher than observed. Generally, in terms of T and S all three models of the present study perform at least as well as the majority of models that contributed to the IPCC AR4 (Meehl et al., 2007; Schneider et al., 2007).

The mixed layer depth (MLD) is a dynamically important variable for upper ocean water mass transport (Gnanadesikan et al., 2002), and especially the maximum (MLD_{max}) during winter time strongly affects the formation of mode, intermediate, deep and bottom waters. Furthermore, ocean mixing plays an important role in surface ocean nutrient availability and thus biological productivity (Najjar et al., 2007). Observation-based estimates of MLD, however, are uncertain, and different methods to determine MLD yield different results for both models and observations (Boyer-Montégut et al., 2004).

MPIM strongly overestimates MLD_{max} in the Southern Ocean, while the other models show too shallow mixing in this area as compared to climatological MLD observations (Boyer-Montégut et al., 2004; Fig. 2). In the low latitudes, all models correspond very

well to the observations, but in the intermediate and high northern latitudes from 20–70° N the models overestimate zonal average MLD_{max} up to a factor of two. Spatial correlations of modelled and observed MLD_{max} are only moderate and on the order of R=0.3–0.4. The tendency towards too deep mixing is expressed by high ratios of normalised standard deviations (std_{mod}/std_{obs}) in a Taylor-diagram (Fig. 1). For MPIM the overestimation of MLD_{max} in the Southern Ocean is known to be caused by too little ice cover in the Weddell Sea (Marsland et al., 2003). This misfit leads to a normalised standard deviation above 6.5 in a Taylor diagram (not shown). However, when applying the definition of MLD as used in Schneider et al. (2007) to temperature and salinity data from the models and the climatological observations (Conkright et al., 2002) the resulting correspondence of MLD_{max} distributions is not considerably better (not shown).

A further approach to assess the modelled ocean circulation fields is a comparison of modelled and observed water mass transports (Schneider et al., 2007; Schmittner et al., 2006; Large et al., 1997). The Atlantic Meridional Overturning Circulation (AMOC) is an important measure for ocean circulation, quantifying the amount of deep waters formed in the North Atlantic, which is of high climatic relevance for the global redistribution of heat and energy by the ocean. In the current study AMOC is defined as the maximum meridional water mass transport below 300 m depth in the North Atlantic, given in Sverdrup (1 Sv=10^6 m^3 s^{-1}). In MPIM the simulated water mass transport lies well within the range of equally defined observation-based estimates for the 1990ies, whereas in IPSL the AMOC is low and in NCAR high, but within the error-bars of one standard deviation both also match the observed range (IPSL: 11.4±1.3 Sv; MPIM: 18.1±0.9 Sv; NCAR: 23.6±1.0 Sv, OBS: 11.5–22.9 Sv; Smethie and Fine, 2001; Talley et al., 2003).

The fully coupled carbon-cycle climate models used in the current study generate their own internal climate variability including coupled ocean-atmosphere modes such as El Nino Southern Oscillation (ENSO). To assess the models' capability to reproduce ENSO variability, the power spectra of SSTs averaged over the Nino3 Box (150° W–90° W, 5° S–5° N) are calculated (Fig. 3). For IPSL and NCAR there are maxima of the

power spectra between two and seven years, which is the typical range of El Nino frequency (Randall et al., 2007), while MPIM does not show a maximum, but also strongly increasing power within this range. This may still be reasonable, as this analysis was performed over a 20 year time-period, which may be too short to exhibit representative ENSO dynamics.

Phosphate concentrations (PO_4) are a good indicator for biogeochemical cycling in the models, as PO_4 is not affected by air-sea gas exchange, which is treated differently in the models. Furthermore, in the current study PO_4 is a fully prognostic tracer in contrast to the models contributing to the OCMIP-2 study, where surface PO_4 was restored (Najjar et al., 2007). The comparison with climatological PO_4 values (Conkright et al., 2002) reveals a good reproduction of annual mean PO_4 fields by all models with correlation coefficients around R~0.85. IPSL and MPIM perform especially very well with normalised standard deviations close to 1 (Fig. 1). For all models the agreement gets weaker when going from the annual mean 3-D distribution of PO_4 to surface water values including the seasonal cycle. Maps of surface water PO_4 concentrations, averaged over the top 0–100 m, show that all models roughly match the general pattern of observed PO_4 distributions with lower values in the oligotrophic subtropical gyres and higher values in the high latitudes, particularly in the Southern Ocean, and also in the equatorial and continental upwelling regions (Fig. 4). MPIM underestimates the surface water PO_4 gradient from high towards low latitudes. The NCAR model overestimates surface PO_4 in the tropical Pacific because excessive iron limitation overly reduces biological phosphate uptake (Fig. 5).

In all models vertically integrated PO_4 concentrations (not shown) are low in the North Atlantic and increase along the conveyor-belt circulation pathway, ending up with a high PO_4 inventory in the North Pacific (Sarmiento et al., 2003). However, all models in general have too high PO_4 concentrations in the North Atlantic. The deviations in the North Pacific PO_4 inventories, which in IPSL and NCAR are too low and in MPIM too high, are probably caused by circulation misfits in the surface water and the thermocline with too weak (IPSL, NCAR) or too strong (MPIM) North Pacific Intermediate Water

formation.

The factors that limit phytoplankton growth in the models are computed from Michaelis-Menten equations for nutrient concentrations, according to MM=N/(N+K), whereby N is the nutrient concentration (PO_4, NO_3, iron and silicate) and K is the respective half-saturation constant as used in each model. The nutrient yielding the lowest MM-value is considered to be the most limiting. Other factors (temperature and light) are assumed to be limiting when MM of the limiting nutrient is still above 0.7. In Fig. 5 the limiting factors are shown when the respective variable is limiting phytoplankton growth during at least one month of the year, showing that in some regions different variables may limit productivity at different times of the year. In the MPIM model iron limitation is even stronger than in NCAR and occurs almost everywhere. In IPSL iron is mostly limiting in the equatorial east Pacific, the Southern Ocean and the North Pacific, which are known to be high nitrate low chlorophyll areas (HNLC) that are strongly iron limited. Furthermore, in IPSL NO_3 is the most limiting factor in the intermediate to low latitudes. In the high latitudes also temperature and light are important for nanophytoplankton growth and diatom production is also limited by the availability of silicate.

In summary, all models show a reasonable agreement with observations of temperature and salinity fields, MLD_{max}, PO_4 concentrations and also with estimates of water mass transports, giving confidence in the models that the simulated circulation fields and biogeochemical cycles are reasonable and comparable to those of other state-of-the-art coupled climate models (Meehl et al., 2007; Randall et al., 2007).

3.2 Annual mean and seasonal cycle of primary productivity and export production

Vertical integrals of PP have been computed over the entire depth of the water column in order to compare with estimates from satellite observations of ocean colour and to derive global integrals for PP (Table 1). In MPIM PP is operationally restricted to 0–90 m and in NCAR to 0–75 m, while in IPSL it can reach below 100 m water depth in the oligotrophic subtropical gyres. The global annual amount of PP ranges from 24 GtC/yr

(MPIM) to 31 GtC/yr (IPSL), and is considerably lower than satellite-based estimates of around 48 GtC/yr (Behrenfeld et al., 2006). Carr et al. (2006) reported a factor of two between global integrals for PP (35–70 GtC/yr) obtained from different algorithms that derive PP from ocean colour, indicating that there is still some uncertainty among those methods. PP from the coupled models is still lower than the low-end satellite estimates. Despite their large spread the different PP algorithms for the observations show patterns of spatial and temporal variability that are similar between different approaches (Carr et al., 2006) and can therefore be used for comparison with results from climate models.

The spatial distributions of modelled PP agree moderately well with the pattern of observation-based PP (Fig. 6). In general, satellite-based and model PP are high in the equatorial upwelling regime, especially the equatorial east Pacific and the equatorial east Atlantic. PP is also elevated in the North Atlantic and the Southern Ocean north of the polar front, while it is low in the subtropical oligotrophic gyres. High PP values as derived from observations for the coastal zones are strongly underestimated by all three models, which is a known fact from coarse resolution models. This underestimation of modelled PP in the coastal regions is mainly responsible for the lower than observed global annual PP. For MPIM and NCAR the fairly low PP suggests that iron limitation in the models is too strong (Fig. 5). In the MPIM model this causes too high PP in the low-latitude Atlantic and too little elsewhere. Furthermore, dust input in MPIM is at the lower end of observed values (Timmreck and Schulz, 2004), leading to low iron deposition from the atmosphere, which further increases the iron stress for marine productivity. The lower PP values in the NCAR model also reflect the fact that the calculated productivity is intermediate between new and primary production, which also partly explains the lower than observed PP values (Fig. 6).

The seasonal variability of PP is shown in Hovmöller diagrams with the zonally averaged PP plotted versus time from observations and models (Fig. 6). Areas of highest productivity are observed in the North Atlantic, where also seasonal variability is highest. In the oligotrophic gyres PP is low throughout the year and variability is also

reduced. Along the equator observed PP has moderate values with low seasonal variability, while in the southern intermediate latitudes (30–50° S) a secondary maximum with high PP and high variability occurs. The models capture the general distribution of higher absolute PP values and higher seasonal variability in the intermediate to high latitudes. IPSL has too high PP values around the equator and too little meridional extension of the oligotrophic gyres. Also in the Southern Ocean PP is overestimated and extending farther southwards than in the observations. In MPIM the periods of high productivity in the higher latitudes are very short, indicating that here PP occurs in very short (strong) pulses, while in the equatorial region PP is higher than the observations with some moderate seasonal variability. The pattern of spatio-temporal variability in NCAR is very similar to the one from the observations, but like in IPSL, PP in the intermediate southern latitudes is biased high and the area of oligotrophic gyres is reduced. The latter is a signal which is arises in the Atlantic, while in the Pacific the expansion of the gyres is too large (Fig. 6).

As mentioned above, the derivation of PP from satellite data entails large uncertainties, as it is a stepwise approach from measurements of ocean colour over the determination of chlorophyll concentrations (and sometimes organic carbon biomass) to PP. While the first steps consider concentrations, PP is a time-dependent rate, requiring even more complicated assumptions about the underlying mechanisms. With each further step from ocean colour to PP the errors propagate, leading to considerable uncertainty in the value of global annual PP, reflected in the factor of 2 spread in the study of Carr et al. (2006). For IPSL, where chlorophyll concentrations are available, a comparison of modelled and satellite-based chlorophyll distributions shows a better agreement than PP values (Fig. 7). Although the model slightly underestimates the surface Chl concentrations, especially in high (northern) latitudes and around the equator, the pattern and the order of magnitude of spatial variability for Chl are slightly closer to observations than those obtained for PP estimates (Fig. 8).

Export Production (EP) describes the amount of particulate organic carbon (POC) that is transported from the surface ocean to depth across a certain depth level (IPSL:

100 m; MPIM: 90 m; NCAR: 75 m). In this study only the material settling through gravitational sinking is regarded, while the total export also encompasses subduction and mixing of suspended particles and dissolved organic matter (DOM) due to water mass transports. The fields of annual mean EP have similar patterns to those of PP for all three models (not shown), i.e. as a first approximation those areas with higher PP also have higher EP. In NCAR this relation is prescribed by using a fixed ratio (1/3) of PP that is exported as POC, while for the other models the amount of EP and its ratio to PP is less straightforward, depending on particle flux and food-web dynamics. The global annual rates of modelled EP are given in Table 1, ranging from 5 GtC/yr (MPIM) to 9 GtC/yr (NCAR), being thus below observation-based estimates reaching from 11 to 22 GtC/yr (Schlitzer, 2000; Laws et al., 2000; Eppley and Peterson, 1979).

Highest EP in IPSL and NCAR occurs in the intermediate to high latitudes between 40–60° North and South, respectively (Fig. 9). A secondary maximum is situated around the equator, where upwelling of nutrient rich deep waters permits high PP (Fig. 6) and thus high EP. Between those areas, in the latitude band of the oligotrophic subtropical gyres (~10–40° North and South) EP is low. In MPIM, zonal average EP increases from low values in the high latitudes to its maximum around the equator, however, in general EP seems to be underestimated everywhere except for the equatorial region if compared to the other models and the observation-based estimates. This distribution will also be caused by the strong iron stress due to too little atmospheric iron deposition (Fig. 5).

In a Taylor diagram the correlation coefficients for the spatial distributions of annual mean EP from the models are rather poor with highest values for IPSL (R=0.35). These correlations are lower than those determined for PP (Fig. 8). One problem for the comparison of different EP estimates are the different reference levels, depending on the definition of EP, as mentioned above. Consequently, the shallowest estimate (NCAR, 75 m) should give highest values and the deepest estimate (Schlitzer, 133 m) lowest export fluxes, which, however, is not the case (Table 1). Another probable reason for the mismatch between modelled and observation-based EP is the large uncertainty of

observation-based estimates for EP. Similar to the PP estimates, they also vary by a factor of two, from global annual mean values of 11 to 22 GtC/yr. Furthermore, the two estimates of Schlitzer (2000) and Laws et al. (2000), which have about the same amount of EP (11 GtC/yr), show very different spatial distributions (Fig. 9) and also spatial correlations between the two are not better than those from comparison with modelled EP (Fig. 8).

3.3 Interannual variability

Primary production is known to be sensitive to climate impacts like for example El Nino Southern Oscillation (ENSO). Consequently, during an El Nino period PP in the tropical Pacific is reduced whereas at a La Nina situation it is enhanced (Behrenfeld et al., 2001; Chavez et al., 1999). From satellite observations it has also been shown that the global signal of interannual PP variability can largely be attributed to the permanently stratified, low-latitude oceans (Behrenfeld et al., 2006). What is more, such anomalies are highly correlated with shifts in the climate system in a way that stronger stratification and the resulting surface ocean warming, which correspond to more El Nino-like conditions, lead to negative PP and chlorophyll anomalies globally over much of the tropics and subtropics. At first sight this relation seems to be counter-intuitive, as phytoplankton growth is positively related to rising temperatures (Eppley, 1972). On the other hand, stronger stratification results in less nutrient supply from deep waters, which in turn limits phytoplankton growth. Algorithms that derive PP from ocean colour make only indirect assumptions about nutrient concentrations via the temperature effect on PP. More detailed answers regardinig the links between stratification, temperature, nutrients and biological productivity can be provided by ocean biogeochemical models. All three models examined in the current study show exactly the same behaviour which was described by Behrenfeld et al. (2006) with the global signal of PP anomalies largely controlled by the permanently stratified low-latitude oceans that have annual average SSTs above 15°C (Fig. 10). It is interesting to see that for all models and the observation-based values the percentage of PP in the low-latitude,

permanently stratified ocean (PP_{strat}) to global PP (PP_{glob}) approximates the fraction of the stratified areas to the global ocean surface area, while the anomalies of PP_{glob} and PP_{strat} are positively correlated (Table 1), which highlights the dominant role of the low-latitude ocean in setting the global signal of PP variability.

Observation-based PP_{strat} anomalies are negatively correlated with changes in stratification and SST over the same area (Fig. 10; Behrenfeld et al., 2006). Note that in interpreting Fig. 10, one should focus on the magnitude and frequency of the PP variability, not the phasing of specific PP events. Because the models are fully coupled, they each generate their own unique internal climate variability that can only statistically be compared with other models and observations. For the model results, a stratification index (SI) was calculated as by Behrenfeld et al. (2006) as the density difference between the sea surface and 200 m water depth. In the IPSL model, PP integrated over the entire domain of the low-latitude, stratified water is strongly anti-correlated with SST and SI. In the NCAR simulation, the biological-physical anti-correlations are more apparent when the analysis is restricted to the area of the Nino3 Box (150–90° W, 5° S–5° N) (Table 2, Fig. 10). For MPIM no correlation can be found between the respective anomalies of PP and stratification (SI) or SST, neither for the whole low-latitude, permanently stratified domain nor for any other individual sub region. This may be due to the fact that in MPIM the equatorial Atlantic ocean is dominated by strongly oscillating predator-prey cycles, which lead to phase shifts in phytoplankton and zooplankton abundance. This can also explain the high amplitude and frequency of interannual variability of PP simulated by MPIM (Fig. 10).

The slopes that can be derived from the anomalies of PP_{strat} versus stratification (SSLOPE) and SST (TSLOPE) are very similar in IPSL and the observation-based estimates (Fig. 11). In the satellite observations for the area of the permanently stratified oceans there is a PP anomaly of –876 TgC/month per unit stratification increase ($kg\,m^{-3}$) and a decrease of –151 TgC/month per degree SST increase (Table 1). For IPSL SSLOPE is slightly weaker (–787 TgC/month) and TSLOPE somewhat stronger (–246 TgC/month). In NCAR both slopes are weaker and correlations insignificant for

the entire low-latitude, stratified domain, but considerably higher correlations are found for the region of the Nino3 Box (Table 2). This area is, however, too small to explain the bulk of the PP variability for the permanently stratified ocean, which governs the global signal in the NCAR simulations. These results indicate that PP variability in NCAR and MPIM, where no good relationship between PP and climate could be detected, acts differently in different areas, summing up to the common signal of the low-latitude, stratified ocean. Mechanisms for PP variability in these two models may be different or different sub regions of the low-latitude stratified ocean may dominate the signal at different times.

A further step is to examine the mechanisms behind the climate-productivity correlations as found in IPSL for the entire low-latitude ocean domain and in NCAR for the tropical East Pacific. As mentioned before, one might expected that PP increases under higher SSTs due to the temperature sensitivity of phytoplankton growh rates (Eppley, 1972). To find out which other mechanisms contribute to PP variability, maps of cross correlations of different anomalies averaged over the whole region (Fig. 12) versus the local PP variability are drawn, highlighting those regions in the models where PP reacts most sensitive to changes in other variables like stratification, SST and surface water nutrient concentrations. Here, the correlation coefficient R^2 is multiplied by the sign of the regression slope to show next to its strength also the direction of the correlation (positive or negative). To isolate the large scale climate impact on productivity "anomalies" of temperature, stratification and nutrient concentrations are averaged over the whole low-latitude, permanently stratified ocean, rather than showing the local signal on each grid-point. The pattern found for anomalies of PP and stratification (SI) in the IPSL model is very similar to the one seen in the observation-based estimates with strongest anti-correlations (negative R^2-values) occurring at the borders of the equatorial tongue (Fig. 12). High positive correlation coefficients (R^2) between PP and (NO_3) concentrations in the same area indicate that stratification and SST changes in the equatorial Pacific lead to changes in the upwelling of nutrients, which further leave their imprint on PP. As the equatorial Pacific is known to be mainly iron limited (Fig. 5),

one would assume to find also a strong impact of iron variability on PP towards the center of the high productivity tongue. The absence of such a signal in IPSL, however, may be caused by the formulation of the iron cycle in IPSL, where iron concentrations are restored to a minimum value of 0.01 nM l^{-1}. By doing so, the natural variability of iron is suppressed, strongly dampening the signal that otherwise would be transferred into PP variability. Furthermore, as iron is strongly scavenged by sinking particles in the surface ocean, the nutricline for iron is deeper than the one for NO_3, so that for iron stronger upwelling is needed to efficiently resupply the surface ocean with iron from below. In NCAR, the highest anti-correlations for PP and SI anomalies are also found in the equatorial Pacific (Fig. 12). Especially for the area of the Nino3 Box higher correlation coefficients between PP and SI/SST than for the entire low-latitude, stratified domain have already been mentioned above. The respective correlation coefficients are given in Table 2, showing also that in NCAR PP in the area of the Nino3 Box is mainly controlled by iron availability, while there is no correlation to PO_4 concentrations. In MPIM there are no considerable correlations between anomalies of PP and PO_4 concentrations, which can be attributed to the effect of too strong iron stress in the model.

From the correlations and the signs of the regression slopes of the variability of PP and SI (stratification index) versus different nutrient concentration anomalies, the chain of cause and effect from climate impacts to nutrient concentrations and further to PP and finally to EP, may be tentatively reconstructed (Table 2). Accordingly, in IPSL the global signal of PP variability is well explained by the behaviour of the entire permanently stratified, low-latitude ocean. Even though in some cases there are moderate correlations between PP and iron variability the slope is negative, which means in the opposite direction than expected (Table 2). This shows the effect of restoring the iron concentrations on hiding the potential impact of iron limitation on PP variability. Instead, PP variability is dominated by NO_3 and PO_4 (Fig. 12, Table 2). Both nutrients show high correlations with climate indicators like SI and SST as well as with PP for the entire stratified, low-latitude domain and also for the Nino3 Box only (Table 2). In MPIM

PP variability is largely independent of PO_4 and other nutrients (Fig. 12), even though the general feature that global PP variability is controlled by the low-latitude oceans is also very well reproduced (Fig. 10). A similar behaviour is found for NCAR, where the North Atlantic also contributes considerably to PP variability (Fig. 6), but this region alone is also not able to explain large parts of the global PP variability. Iron is the main limiting nutrient for productivity in the low latitudes of the NCAR model (Fig. 5), and especially in the area of the Nino3 Box there are high correlation coefficients between stratification, SST and iron variability and further on for iron and PP variability (Table 2). One reason for the absence of a higher correlation between the anomalies of PP and nutrients of the whole low-latitude area maybe the fact that in the NCAR model PP stands for net nutrient uptake, which includes processes like grazing and heterotrophic respiration.

The pattern of the sensitivity of PP to climate is transferred into EP variability. EP reacts most sensitive to changes in PP in those areas, where PP reacts most to climate variability (Fig. 13). In IPSL, variability in EP is strongly correlated with the average PP variability at the borders of the high productivity tongue in the equatorial Pacific, a pattern which is also reproduced by the EP correlations with NO_3 anomalies (Fig. 13). In MPIM there are no considerable correlations between EP and PP or other climate and nutrient anomalies when regarding the entire low-latitude ocean. In the NCAR model, EP shows the strongest correlation with PP variability in the North Atlantic, where PP (and thus EP) exhibits the strongest interannual variability. Correlation coefficients different from 1 can be found, even though EP is fixed to be 1/3 of PP, as local EP variability is correlated with PP variability averaged over the entire low-latitude, permanently stratified domain. For the global integrals of PP and EP, however, the correlation is 1 (Table 2). Surprisingly, neither IPSL nor NCAR show considerable correlations of EP with changes in the mixed layer depth.

4 Conclusions

The current study has shown that while it is still difficult to reproduce absolute values of observation-based annual mean PP with ocean biogeochemical models, both the mechanisms and the amount of interannual variability are well captured by the models. In good agreement with recent satellite observations, the global signal of modelled PP variability is largely dominated by the low-latitude, permanently stratified ocean (Behrenfeld et al., 2006). This result is very robust across the models, even though they perform differently in representing biogeochemical cycles (Fig. 5). The finding of the dominating role of PP in the low-latitude ocean, however, has also be regarded with some care, as both 3-D models and satellite observations may be biased towards lower latitudes. High-latitude satellite-derived PP values especially for the Southern Ocean are less well constrained than those for the low-latitudes due to cloud coverage and the poorer availability of reference measurements. The 3-D coupled models are sometimes tuned to reproduce climate and biogeochemical variability in the low latitudes, while in the high latitudes difficulties with sea-ice interactions may occur.

In particular, in this study we are able to demonstrate that under more El Nino-like conditions with surface ocean warming and stronger stratification in the low-latitude ocean, nutrient supply to the surface ocean is reduced, and results in lower PP and EP. In a future warming climate with permanent El Nino like conditions both PP and EP probably will be reduced, which has already been shown by other climate model simulations (Sarmiento et al., 2004; Boyd and Doney, 2002; Bopp et al., 2001). TSLOPE was determined in the present study from observation-based estimates and the IPSL model to quantify PP sensitivity to SST (Table 2). As the model simulations were run until the year 2100 using the A2 scenario, results are available to check whether TSLOPE also holds for the future impact of climate change on PP in the low-latitude ocean. Accordingly, one would expect PP (EP) in the low-latitude ocean to decrease by 3 GtC/yr (0.6 GtC/yr) per 1°C temperature increase. For this particular area the IPSL model predicts an increase of the average SST of 1.6°C from the years 1985–2005 until

2090–2099. This should lead to a decrease in PP (EP) by 4.8 GtC/yr (1 GtC/yr), which amounts to a decline of 27%. However, the model predicts PP over the same time period and area to reduce only by 1.6 GtC/yr (–9%) and EP by 0.7 GtC/yr (–19%). This shows that TSLOPE, which was derived from modelled interannual variability during the two decades between 1985 and 2005, can not be used for extrapolation into future climate conditions. Consequently, to estimate the impact of future climate change on marine productivity further mechanisms and, of course, also the high latitude ocean will have to be considered, which will be done in a complementary study that analyses the continuation of the here presented model simulations in a scenario of future climate change (SRES A2) until the year 2100.

In summary, the current study has illustrated a strong link between marine productivity and climate variability, both derived from satellite observations, with coupled climate carbon cycle modelling. On the one hand observation-based estimates have been used to constrain model results for ocean circulation and biogeochemical cycling, while on the other hand results from the climate models have been used to interpret and reconstruct the mechanisms that underly climate-driven shifts in marine productivity that have been observed. The strong agreement between the areas and mechanisms that dominate PP variability on the global scale for both types of investigation increases confidence in results obtained by both models and observation-based estimates, and it demonstrates the power and importance of model data intercomparisons on the way to better understand the links between climate and marine biogeochemical cycles.

Acknowledgements. We thank I. Fung and K. Lindsay for their work contributing to the set up of the NCAR model and A. Tagliabue for his comments on the manuscript. This work was supported by the EU grants 511106-2 (FP6 RTD project EUR-OCEANS) and GOCE-511176 (FP6 RTP project CARBOOCEAN) by the European Comission. This is publication number 2548 from LSCE.

References

Aumont, O. and Bopp, L.: Globalizing results from ocean in situ iron fertilization studies, Global Biogeochem. Cycles, 20, GB2017, doi:10.1029/2005GB002591, 2006.

Aumont, O., Maier-Reimer, E., Blain, S., and Monfray, P.: An ecosystem model of the global ocean including Fe, Si, P colimitations, Global Biogeochem. Cycles, 17(2), 1060, doi:10.1029/2001GB001745, 2003.

Behrenfeld, M. and Falkowski, P.: Photosynthetic rates derived from satellite-based chlorophyll concentration, Limnol. Oceanogr., 42, 1–20, 1997.

Behrenfeld, M. J., Randerson, J. T., McClain, C. R., Feldman, G. C., Los, S. O., Tucker, C. J., Falkowski, P. G., Field, C. B., Frouin, R., Esaias, W. E., Kolber, D. D., and Pollack, N. H.: Biospheric Primary Production during an ENSO Transition, Science, 291, 2594–2597, 2001.

Behrenfeld, M. J., Boss, E., Siegel, D. A., and Shea, D. M.: Carbon-based ocean productivity and phytoplankton physiology from space, Global Biogeochem. Cycles, 19, GB1006, doi:10.1029/2004GB002299, 2005.

Behrenfeld, M. J., O'Malley, R. T., Siegel, D. A., McClain, C. R., Sarmiento, J. L., Feldman, G. C., Milligan, A. J., Falkowski, P. G., Letelier, R. M., and Boss, E. S.: Climate-driven trends in contemporary ocean productivity, Nature, 444, 752–755, 2006.

Bopp, L., Monfray, P., Aumont, O., Dufresne, J. L., Le Treut, H., Madec, G., Terray, L., and Orr, J. C.: Potential impact of climate change on marine export production, Global Biogeochem. Cycles, 15, 81–99, 2001.

Bopp, L., Aumont, O., Cadule, P., Alvain, S., and Gehlen, M.: Response of diatoms distribution to global warming and potential implications: A global model study, Geophys. Res. Lett., 32, L19606, doi:10.1029/2005GL023653, 2005.

Boville, B. A. and Gent, P.: The NCAR Climate System Model, version one., J. Climate, 11, 1115–1130, 1998.

Boville, B. A., Kiehl, J., Rasch, P., and Bryan, F.: Improvements to the NCAR CSM-1 for transient climate simulations, J. Climate, 13, D02S070, doi:10.1029/2002JD003026, 2001.

Boyd, P. W. and Doney, S. C.: Modelling regional responses by marine pelagic ecosystems to global climate change, Geophys. Res. Lett., 29(16), 1806, doi:10.1029/2001GL014130, 2002.

Boyer-Montégut, C., Madec, G., Fischer, A. S., Lazar, A., and Iudicone, D.: Mixed layer depth over the global ocean: An examination of profile data and a profile-based climatology, J.

Geophys. Res., 109, C12003, doi:10.1029/2004JC002378, 2004.

Carr, M.-E., Friedrichs, M. A. M., Schmeltz, M., Noguchie Aita, M., Antoine, D., Arrigo, K. R., Asanuma, I., Aumont, O., Barber, R., Behrenfeld, M., Bidigare, R., Buitenhuis, E. T., Campbell, J., Ciotti, A., Dierssen, H., Dowell, M., Dunne, J., Esaias, W., Gentili, B., Gregg, W., Groom, S., Hoepffner, N., Ishizaka, J., Kameda, T., Le Quéré, C., Lohrenz, S., Marra, J., Mélin, F., Moore, K., Morel, A., Reddy, T. E., Ryan, J., Scardi, M., Smyth, T., Turpie, K., Tilstone, G., Waters, K., and Yamanaka, Y.: A comparison of global estimates of marine primary production from ocean color, Deep-Sea Res., 53, 741–770, 2006.

Chavez, F. P., Strutton, P. G., Friederich, G. E., Feely, R. A., Feldman, G. C., Foley, D. G., and McPhaden, M. J.: Biological and Chemical Response of the Equatorial Pacific Ocean to the 1997–98 El Nino, Science, 286, 2126–2131, 1999.

Collier, M. A. and Durack, P. J.: CSIRO netCDF version of the NODC World Ocean Atlas 2005, Marine and Atmospheric Research Paper 15, CSIRO, Victoria, Australia, p. 1–45, 2006.

Conkright, M. E., Locarnini, R. A., Garcia, H. E., O'Brien, T. D., Boyer, T. P., Stephens, C., and Antonov, J. I.: World Ocean Atlas 2001: Objective Analyses, Data Statistics, and Figures, CD-ROM documentation, NOAA, Silver Spring, 2002.

Doney, S. C., Lindsay, K., Caldeira, K., Campin, J.-M., Drange, H., Dutay, J.-C., Follows, M., Gao, Y., Gnanadesikan, A., Gruber, N., Ichida, A., Joos, F., Madec, G., Maier-Reimer, E., Marshall, J. C., Matear, R. J., Monfray, P., Mouchet, A., Najjar, R., Orr, J. C., Plattner, G. K., Sarmiento, J., Schlitzer, R., Slater, R., Totterdell, I. J., Weirig, M. F., Yamanaka, Y., and Yool, A.: Evaluating global ocean carbon models: the importance of realistic physics, Global Biogeochem. Cycles, 18, GB3017, doi:10.1029/2003GB002150, 2004.

Doney, S. C., Lindsay, K., Fung, I., and John, J.: Natural variability in a stable, 1000-Yr global coupled climate-carbon cycle simulation, J. Climate, 19, 3033–3054, 2006.

Eppley, R. W.: Temperature and phytoplankton growth in the sea, Fishery Bulletin, 70, 1063–1085, 1972.

Eppley, R. W. and Peterson, B. J.: Particulate organic matter flux and planktonic new production in the deep ocean, Nature, 282, 677–680, 1979.

Friedlingstein, P., Cox, P., Betts, R., Bopp, L., von Bloh, W., Brovkin, V., Cadule, P., Doney, S., Eby, M., Fung, I., Bala, G., John, J., Jones, C., Joos, F., Kato, T., Kawamiya, M., Knorr, W., Lindsay, K., Matthews, H. D., Raddatz, T., Rayner, P., Reick, C., Roeckner, E., Schnitzler, K.-G., Schnur, R., Strassmann, K., Weaver, A. J., Yoshikawa, C., and Zeng, N.: Climate-Carbon Cycle Feedback Analysis: Results from the C^4 MIP Model Intercomparison, J. Climate, 19,

3337–3353, 2006.
Gehlen, M., Bopp, L., Emprin, N., Aumont, O., Heinze, C., and Ragueneau, O.: Reconciling surface ocean productivity, export fluxes and sediment composition in a global biogeochemical ocean model, Biogeosciences, 3, 521–537, 2006, http://www.biogeosciences.net/3/521/2006/.
Gent, P. R., Bryan, F. O., Danabasoglu, G., Doney, S. C., Holland, W. R., Large, W. G., and McWilliams, J. C.: The NCAR Climate System Model global ocean component, J. Climate, 11, 1287–1306, 1998.
Gnanadesikan, A., Slater, R. D., Gruber, N., and Sarmiento, J.: Oceanic vertical exchange and new production: a comparison between models and observations, Deep-Sea Res. II, 49, 363–401, 2002.
Hourdin, F., Musat, I., Bony, S., Braconnot, P., Codron, F., Dufresne, J.-L., Fairhead, L., Filiberti, M.-A., Friedlingstein, P., Grandpeix, J.-Y., Krinner, G., LeVan, P., Li, Z.-X., and Lott, F.: The LMDZ4 general circulation model: climate performance and sensitivity to parametrized physics with emphasis on tropical convection, Clim. Dynam., 19, 3445–3482, doi:10.1007/s00382-006-0158-0, 2006.
Joos, F., Plattner, G. K., Stocker, T. F., Marchal, O., and Schmittner, A.: Global Warming and Marine Carbon Cycle Feedbacks on Future Atmospheric CO_2, Science, 284, 464–467, 1999.
Kiehl, J., Hack, J., Bonan, G., Boville, B., Williamson, D., and Rasch, P.: The National Center for Atmospheric Research Community Climate Model, J. Climate, 11, 1151–1178, 1998.
Krinner, G., Viovy, N., deNoblet-Ducoudré, N., Ogée, J., Polcher, J., Friedlingstein, P., Ciais, P., Sitch, S., and Prentice, C.: A dynamic global vegetation model for studies of the coupled atmosphere-biosphere system, Global Biogeochem. Cycles, 19, GB1015, doi: 10.1029/2003GB002199, 2005.
Large, W. G., Danabasoglu, G., Doney, S. C., and McWilliams, J. C.: Sensitivity to surface forcing and boundary layer mixing in a global ocean model: annual-mean climatology, J. Phys. Oceanogr., 27, 2418–2447, 1997.
Laws, E. A., Falkowski, P. G., Smith, W. O., and Ducklow, H.: Temperature effects on export production in the open ocean, Global Biogeochem. Cycles, 14, 1231–1246, 2000.
Madec, G., Delecluse, P., Imbard, M., and Lévy, M.: OPA 8.1 ocean general circulation model reference manual, Notes du Pôle de Modélisation 11, Tech. rep., IPSL, Paris, 1–91, 1998.
Maier-Reimer, E.: Geochemical cycles in an ocean general circultion model. Preindustrial

tracer distributions, Global Biogeochem. Cycles, 7, 645–677, 1993.
Maier-Reimer, E., Mikolajewicz, U., and Winguth, A.: Future ocean uptake of CO_2: interaction between ocean circulation and biology, Clim. Dynam., 12, 63–90, 1996.
Maier-Reimer, E., Kriest, I., Segschneider, J., and Wetzel, P.: The HAMburg Ocean Carbon Cycle model HAMOCC5.1 – Technical description., Berichte zur Erdsystemforschung 14/2005 14, Max Planck-Institut für Meteorologie, Hamburg, Germany, available at http://www.mpimet.mpg.de, 2005.
Marsland, S. J., Haak, H., Jungclaus, J. H., Latif, M., and Röske, F. R.: The Max-Planck-Institute global ocean/sea ice model with orthogonal curvilinear coordinates, Ocean Model., 5, 91–127, 2003.
Meehl, G. A., Stocker, T. F., Collins, W. D., Friedlingstein, P., Gaye, A. T., Gregory, J. M., Kitoh, A., Knutti, R., Murhpy, M., Noda, A., Raper, S. C. B., Watterson, I. G., Weaver, A. J., and Zhao, Z. C.: Global Climate Projections, in: Climate Change 2007: The Physical Science Basis, Contribution of Working Group I to the Fourth Assessment Report of the Intergovernmental Panel on Climate Change, edited by: Solomon, S., Quin, D., Manning, M., Chen, Z., Marquis, M., Averyt, K. B., Tignor, M., and Miller, H. L., Cambridge University Press, Cambridge, United Kingdom and New York, NY, USA, 747–845, 2007.
Najjar, R. G., Jin, X., Louanchi, F., Aumont, O., Caldeira, K., Doney, S. C., Dutay, J.-C., Follows, M., Gruber, N., Joos, F., Lindsay, K., Maier-Reimer, E., Matear, R. J., Matsumoto, K., Monfray, P., Mouchet, A., Orr, J. C., Plattner, G. K., Sarmiento, J. L., Schlitzer, R., Weirig, M. F., Yamanaka, Y., and Yool, A.: Impact of circulation on export production, dissolved organic matter and dissolved oxygen in the ocean: Results from OCMIP-2, Global Biogeochem. Cycles, in press, 2007.
Oschlies, A. and Kähler, P.: Biotic contribution to air-sea fluxes of CO_2 and O_2 and its relation to new production, export production, and net community production, Global Biogeochem. Cycles, 18, GB1015, doi:10.1029/2003GB002094, 2004.
Plattner, G.-K., Joos, F., Stocker, T. F., and Marchal, O.: Feedback mechanisms and sensitivities of ocean carbon uptake under global warming, Tellus, 53B, 564–592, 2001.
Randall, D. A., Wood, R. A., Bony, S., Colman, R., Fichefet, T., Fyfe, J., Kattsov, V., Pitman, A., Shukla, J., Srinivasan, J., Stouffer, R. J., Sumi, A., and Taylor, K. E.: Climate Models and Their Evaluation, in: Climate Change 2007: The Physical Science Basis, Contribution of Working Group I to the Fourth Assessment Report of the Intergovernmental Panel on Climate Change, edited by: Solomon, S., Quin, D., Manning, M., Chen, Z., Marquis, M.,

Averyt, K. B., Tignor, M., and Miller, H. L., Cambridge University Press, Cambridge, United Kingdom and New York, NY, USA, 598–662, 2007.

Randerson, J. T., Thompson, M. V., Conway, T. J., Fung, I. Y., and Field, C. B.: The contribution of terrestrial sources and sinks to trends in the seasonal cycle of atmospheric carbon dioxide, Global Biogeochem. Cycles, 11, 535–560, 1997.

Roeckner, E., Brokopf, R., Esch, M., Giorgetta, M., Hagemann, S., Kornblueh, L., Manzini, E., Schlese, U., and Schulzweida, U.: Sensitivity of simulated climate to horizontal and vertical resolution in the ECHAM5 atmosphere model, J. Climate, 19, 3771–3791, 2006.

Sarmiento, J. L., Gruber, N., Brzezinski, M. A., and Dunne, J. P.: High-latitude controls of thermocline nutrients and low latitude biological productivity, Nature, 427, 56–60, 2003.

Sarmiento, J. L., Slater, R., Barber, R., Bopp, L., Doney, S. C., Hirst, A. C., Kleypas, J., Matear, R., Mikolajewicz, U., Monfray, P., Soldatov, V., Spall, S. A., and Stouffer, R.: Response of ocean ecosystems to climate warming, Global Biogeochem. Cycles, 18, doi: 10.1029/2003GB002134, GB3003, 2004.

Schlitzer, R.: Applying the Adjoint Method for Global Biogeochemical Modeling, in: Inverse Methods in Biogeochemical Cycles, edited by: Kasibhatla, P., Heimann, M., Hartley, D., Mahowald, N., Prinn, R., and Rayner, P., 107–124, AGU, USA, 2000.

Schmittner, A., Latif, M., and Schneider, B.: Model projections of the North Atlantic thermohaline circulation for the 21st century assessed by observations, Geophys. Res. Lett., 32,L23710, doi:10.1029/2005GL024368, 2005.

Schneider, B., Latif, M., and Schmittner, A.: Evaluation of Different Methods to Assess Model Projections of the Future Evolution of the Atlantic Meridional Overturning Circulation, J. Climate, 20, 2121–2132, doi:10.1175/JCLI4128.1, 2007.

Smethie, W. M. and Fine, R. A.: Rates of North Atlantic Deep Water formation calculated from chlorofluorocarbon inventories, Deep-Sea Res. I, 48, 189–215, 2001.

Solomon, S., Qin, D., Manning, M., Alley, R. B., Berntsen, T., Bindoff, N. L., Chen, Z., Chidthaisong, A., Gregory, J. M., Hegerl, G. C., Heimann, M., Hewitson, B., Hoskins, B. J., Joos, F., Jouzel, J., Kattsov, V., Lohmann, U., Matsuno, T., Molina, M., Nicholls, N., Overpeck, J., Raga, G., Ramaswamy, V., Ren, J., Rusticucci, M., Somerville, R., Stocker, T. F., Whetton, P., Wood, R., and Wratt, D.: Technical Summary, in: Climate Change 2007: The Physical Science Basis, Contribution of Working Group I to the Fourth Assessment Report of the Intergovernmental Panel on Climate Change edited by: Solomon, S., Qin, D., Manning, M., Chen, Z., Marquis, M., Averyt, K. B., Tignor, M., and Miller, H. L., Cambridge University

Press, Cambridge, United Kingdom and New York, NY, USA, 1–91, 2007.

Talley, L. D., Reid, J. L., and Robbins, P. E.: Data-based meridional overturning streamfunctions for the global ocean, J. Climate, 19, 3213–3226, 2003.

Timmreck, C. and Schulz, M.: Significant dust simulation differences in nudged and climatological operation mode of the AOGCM ECHAM, J. Geophys. Res., 109, D13202, doi: 10.1029/2003JD004381, 2004.

Volk, T. and Hoffert, M. I.: Ocean carbon pumps: analysis of relative strengths and efficiencies in ocean-driven atmospheric CO_2 changes, in: The carbon cycle and atmospheric CO_2: natural variations Archean to Present, edited by: Sundquist, E. and Broecker, W. S., no. 32 in Geophys. Monograph, 99–110, AGU, Washington D.C., 1985.

Table 1. Depth integrated net primary production (PP) and Export of POC (EP) for the different models and observation-based estimates. PP_{glob}: global annual PP; PP_{strat}: global annual PP in the area of the permanently stratified, low-latitude ocean; $Area_{strat}$: percentage of the permanently stratified, low-latitude ocean to the global ocean domain; R^2 PP_{ano} correlation coefficient for anomalies of PP_{glob} versus anomalies of PP_{strat}; $SSLOPE_{PP}$: slope of the regression line for PP_{ano} (=difference of monthly PP value to the climatological mean of PP) and SI_{ano} (=difference of monthly stratification value to climatological mean stratification); R^2 $SSLOPE_{PP}$: correlation coefficient for PP_{ano} and SI_{ano}; $TSLOPE_{PP}$: slope of the regression line for PP_{ano} and SST_{ano}; R^2 $TSLOPE_{PP}$: correlation coefficient for PP_{ano} and SST_{ano}. Notation for EP correlations is equivalent. Values in brackets correspond to one standard deviation.

Primary Production	IPSL	MPIM	NCAR	SEAWIFS	
PP_{glob} (GtC yr^{-1})	30.7 (3.1)	23.7 (8.6)	27.4 (3.3)	47.5 (2.4)	
PP_{strat} (GtC yr^{-1})	17.7 (1.8)	17.7 (3.4)	17.8 (2.2)	34.6 [1] (1.3)	
PP_{strat} (%)	58	75	65	73[1]	
$Area_{strat}$ (%)	62	67	66	72[1]	
R^2 PP_{ano}	0.88	0.85	0.78	0.69[1]	
$SSLOPE_{PP}$ (TgC kg^{-1} m^{-3})	–787	0	–143	–876	
R^2 $SSLOPE_{PP}$	0.70	0.04	0.02	0.69	
$TSLOPE_{PP}$ (TgC°C^{-1})	–246	0	–65	–151	
R^2 $TSLOPE_{PP}$	0.67	0.03	0.05	0.85	
POC Export	**IPSL**	**MPIM**	**NCAR**	**Schlitzer**	**Laws**
EP_{glob} (GtC yr^{-1})	8.6 (0.8)	5.0 (1.8)	9.0 (1.1)	11.4	11.1
EP_{strat} (GtC yr^{-1})	3.6 (0.3)	3.8 (0.7)	5.6 (0.7)	7.0[1]	6.2[1]
EP_{strat} (%)	42	75	62	61[1]	56[1]
R^2 EP_{ano}	0.65	0.91	0.78		
$SSLOPE_{EP}$ (TgC kg^{-1} m^{-3})	–184	0	–57		
R^2 $SSLOPE_{EP}$	0.61	0.04	0.03		
$TSLOPE_{EP}$ (TgC°C^{-1})	–47	0	–23		
R^2 $TSLOPE_{EP}$	0.61	0.04	0.06		

[1] SST data from Conkright et al. (2002).

Table 2. Correlation coefficients (R^2) and signs of regression slopes (+/–) of cross correlations of local anomalies of PP and stratification (SI) versus the anomalies of different variables averaged over the area of the low-latitude, stratified ocean (LL-STRAT) and the Nino3 Box (NINO3; 150° W–90° W, 5° S–5° N).

		IPSL				**MPIM**				**NCAR**			
		LL-STRAT		NINO3		LL-STRAT		NINO3		LL-STRAT		NINO3	
		R^2	+/–	R^2	+/–	R^2	+/–	R^2	+/–	R^2	+/–	R^2	+/–
PP	SI	0.70	–	0.86	–	0.04	–	0.01	–	0.02	–	0.54	–
	SST	0.67	–	0.85	–	0.03	–	0.06	–	0.05	–	0.66	–
	Iron	0.37	–	0.50	–	0.06	–	0.21	–	0.10	–	0.64	+
	PO_4	0.67	+	0.82	+	0.01	+	0.01	–	0.00	+	0.00	+
	NO_3	0.68	+	0.76	+	0.01	+	0.01	+				
	EP	0.73	+	0.87	+	0.18	+	0.18	+	1.00	+	1.00	+
SI	SST	0.95	+	0.97	+	0.91	+	0.92	+	0.81	+	0.92	+
	Iron	0.59	+	0.59	+	0.04	–	0.32	–	0.04	+	0.78	–
	PO_4	0.70	–	0.86	–	0.42	–	0.49	–	0.01	–	0.00	–
	NO_3	0.58	–	0.78	–	0.50	–	0.45	–				
	EP	0.61	–	0.79	–	0.04	–	0.01	–	0.03	–	0.59	–

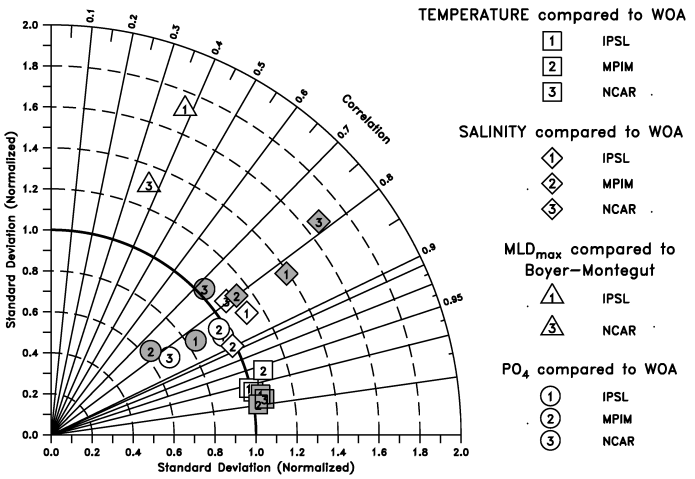

Fig. 1. Taylor diagram showing the correspondence between model results and observations for 3-D fields of annual mean temperature (squares) and salinity (diamonds), 2-D fields of MLD_{max} (triangles) and 3-D fields of annual mean PO_4 concentration (circles). Grey symbols for T and S show spatial correlations for sea surface temperature (SST) and sea surface salinity (SSS) including the seasonal cycle, grey symbols for PO_4 represent average surface water (0–100 m) PO_4 concentrations, also including the seasonal cycle (WOA: World Ocean Atlas). For MLD_{max} in MPIM the normalised standard deviation is 6.5 (not shown here). The radial coordinate indicates correlation coefficients (R), the x and y-axes show normalised standard deviations (std_{model}/std_{obs}). A model perfectly matching the observations would reside in point (1,1).

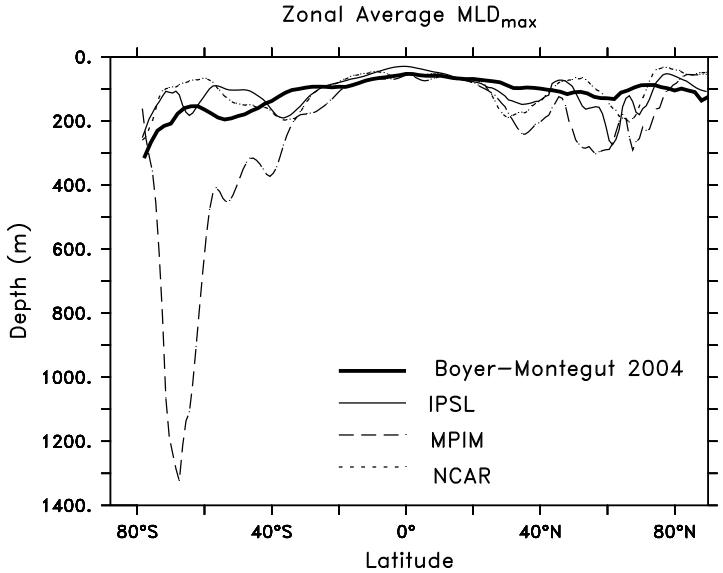

Fig. 2. Modelled and observed climatological zonal average MLD_{max}.

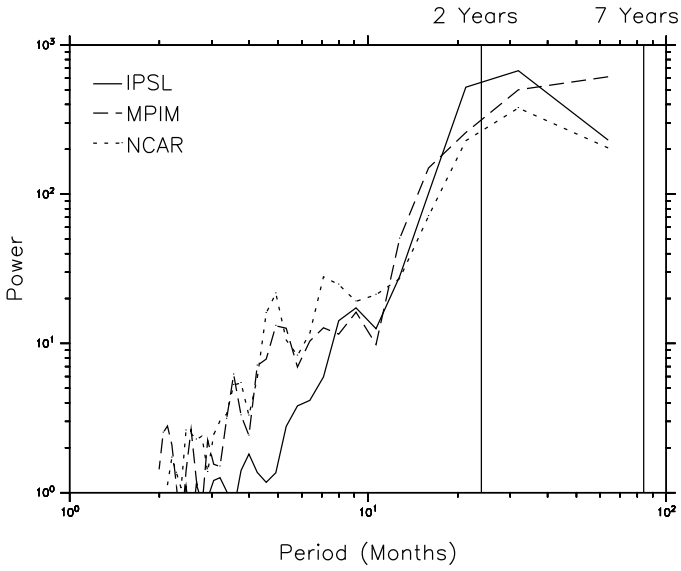

Fig. 3. Maximum entropy power spectra of modelled sea surface temperatures (SST) averaged over the Nino3 Box (150° W–90° W, 5° S–5° N). The vertical lines correspond to periods of two and seven years, respectively, corresponding to the typical range of ENSO frequency.

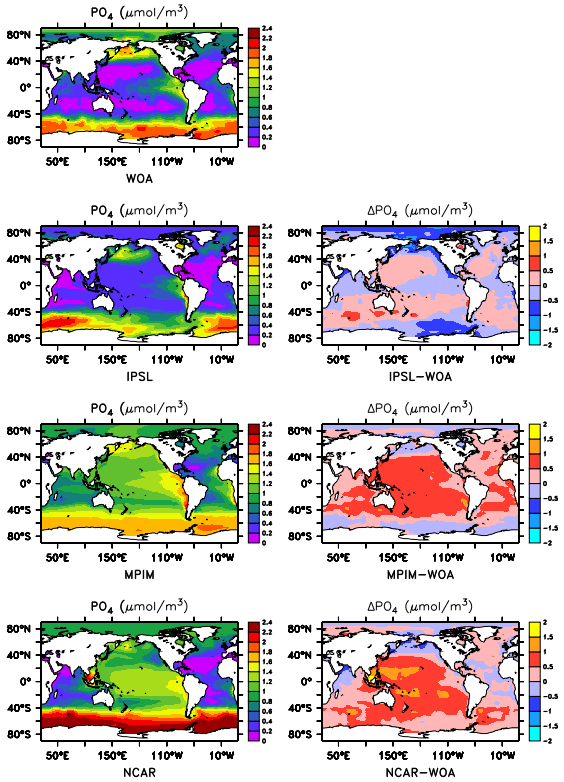

Fig. 4. Maps of observed (top left) and modelled (left column) surface water PO_4 concentrations, averaged over the top 0–100 m of the water column. Right column: Model minus observation difference of surface water PO_4 concentrations (WOA: World Ocean Atlas).

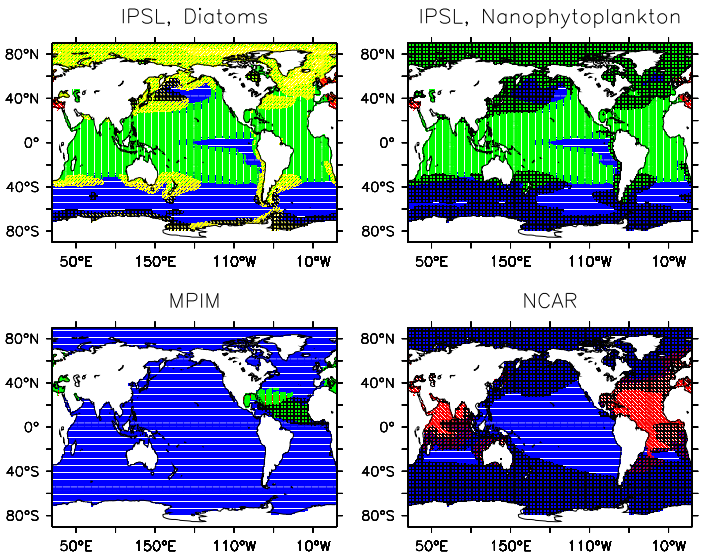

Fig. 5. Maps of variables limiting phytoplankton growth in the models. Blue: iron; red: PO_4; green: NO_3; yellow: silicate; black: temperature and light. Shown are areas where the respective variable is limiting during at least one month of the year. For nutrients the respective most limiting nutrient is shown, while limitation due to other factors (temperature + light) is shown when nutrients are not limiting, which means the value of the Michaelis-Menten term is above 0.7 (see explanations in the text).

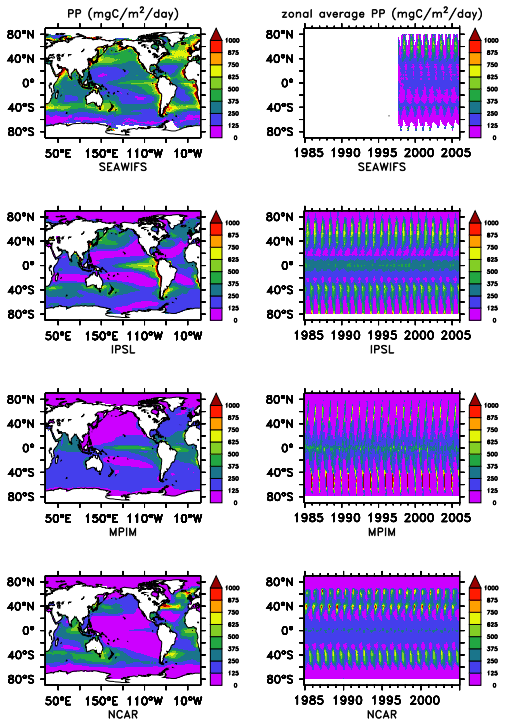

Fig. 6. Left column: maps of observation-based (top) and modelled (others) vertically integrated primary production (PP). Right column: Hovmöller diagrams showing the seasonal variability of vertically integrated PP.

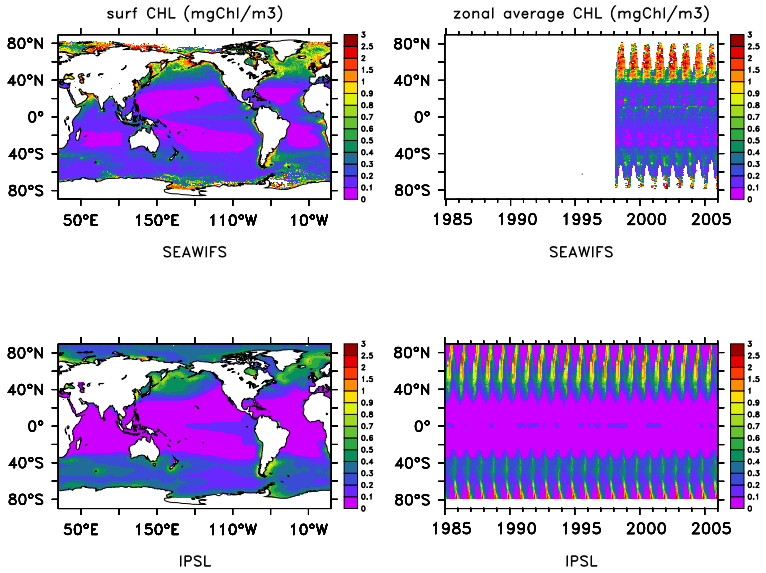

Fig. 7. Left column: maps of surface water chlorophyll concentrations based on observations (top) and modelled (bottom). Right column: Hovmöller diagrams showing the seasonal variability of surface water chlorophyll concentrations.

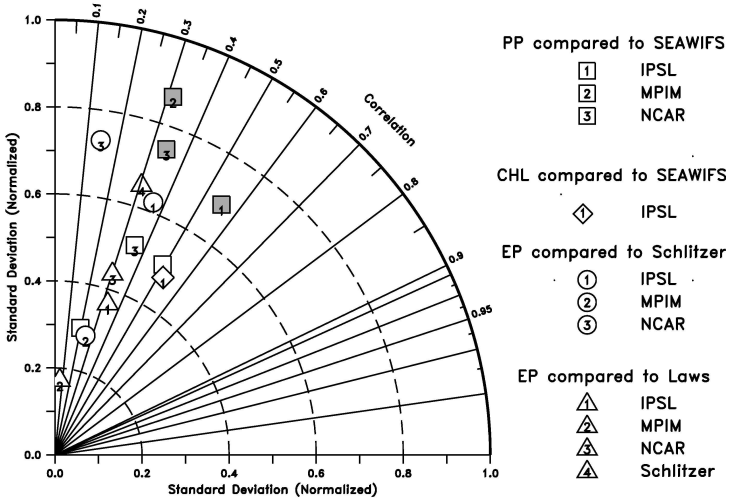

Fig. 8. Taylor diagram showing the correspondence between model results and observation-based estimates for primary production (PP), chlorophyll and export production (EP). White symbols show results for annual mean 2-D fields, grey symbols include the seasonal cycle for PP. The radial coordinate indicates correlation coefficients (R), the x and y-axes show normalised standard deviations (std_{model}/std_{obs}). A model perfectly matching the observations would reside in point (1,1).

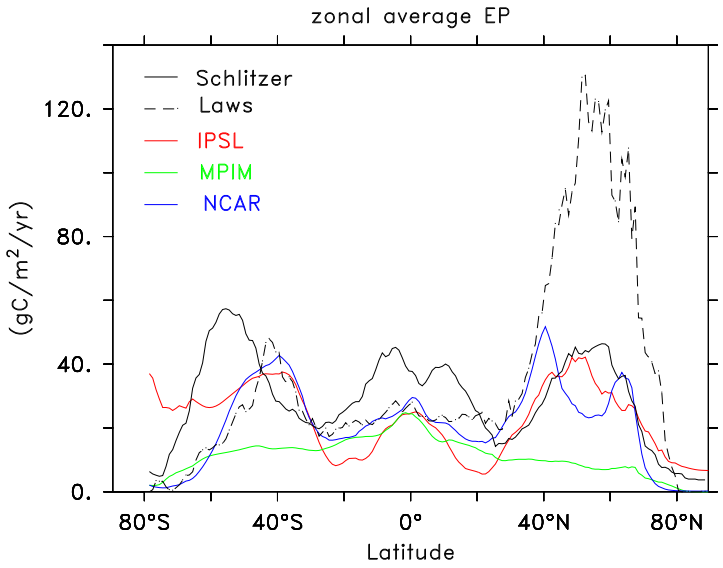

Fig. 9. Zonal average export production (EP) from models and observation-based estimates. Please note that the different estimates refer to different depths (Schlitzer 133 m; Laws 100 m; IPSL 100 m; MPIM 90 m; NCAR 75 m.

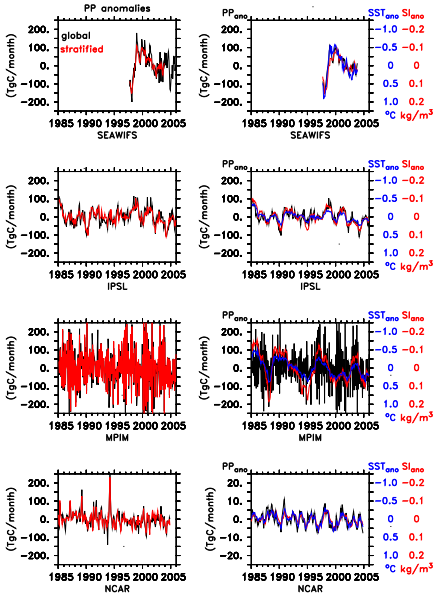

Fig. 10. Left column: timeseries of observation-based (top) and modelled (others) primary production (PP) anomalies for the global (black) and the low-latitude, permanently stratified ocean (red), which has annual mean SSTs above 15°C. The anomalies are calculated as the difference in the actual monthly PP value to the climatological mean of the corresponding month. Right column: timeseries of the observation-based (top) and modelled (others) PP anomalies for the permanently stratified ocean (black) overlain by anomalies for stratification (red) and SST (blue). For the NCAR model results from the Nino3-Box are displayed, which yields PP anomalies which are an order of magnitude lower than for the global and the low-latitude cases. Please note that the scales for the latter two indices (SI, SST) have been inverted.

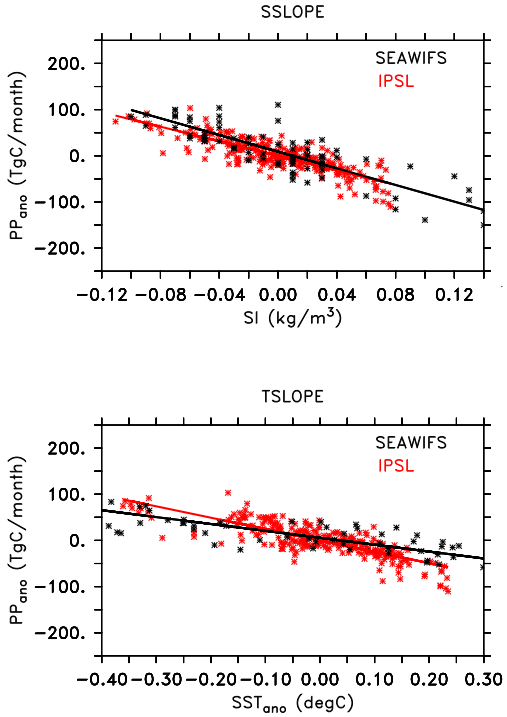

Fig. 11. Top: Scatter plot of modelled and observation-based anomalies for stratification and primary production (PP). Bottom: Scatter plot of modelled and observed anomalies for SST and PP. Slopes and correlation coefficients for the regression lines are given in Table 1.

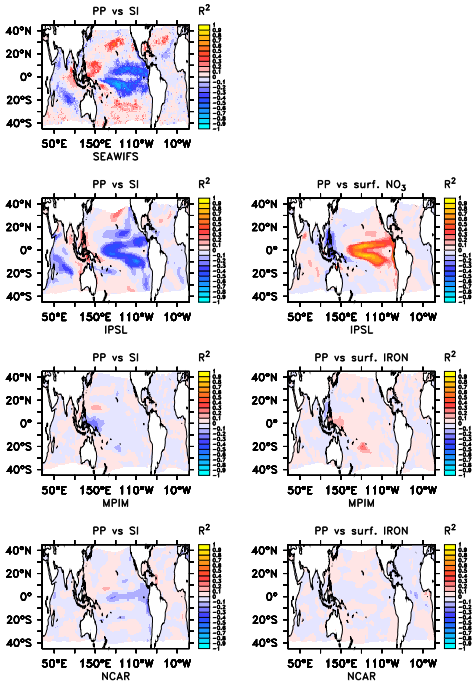

Fig. 12. Maps of cross correlation coefficients (R^2) of modelled and observation-based local primary production (PP) anomalies versus variability of stratification and different nutrient concentrations averaged over the respective shaded area. The R^2-values have been multiplied with the sign of the regression slope, so that positive (red) values for R^2 indicate positive correlations, negative (blue) values show anti-correlations. Please note that in the right column PP is correlated with different nutrient concentrations, which are the most limiting for the respective model (see also Fig. 5).

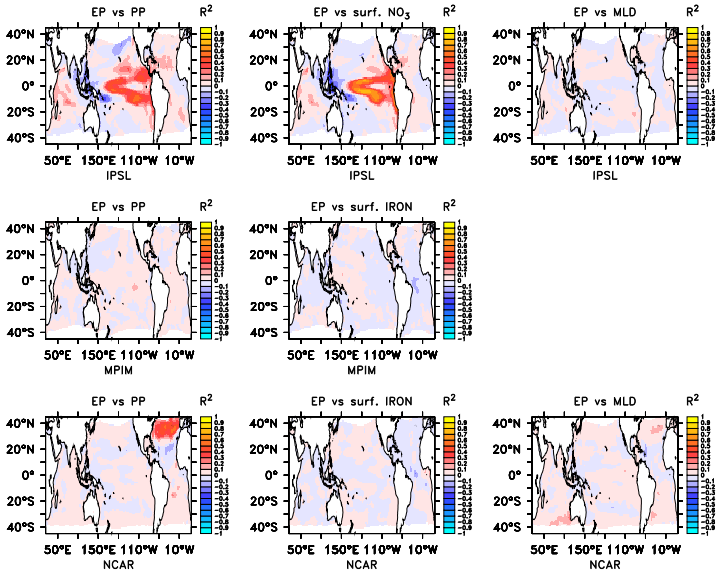

Fig. 13. Maps of modelled cross correlation coefficients of local export production (EP) anomalies versus variability in primary production (PP), different nutrients and MLD averaged over the respective shaded areas. The R^2-values have been multiplied with the sign of the regression slope, so that positive (red) values for R^2 indicate positive correlations, negative (blue) values show anti-correlations. Please note that in the middle column EP is correlated with different nutrient concentrations, which are the most limiting for the respective model (see also Fig. 5).